Research Repository UCD

Title	Magnetic ferrite/carbonized cotton fiber composites for improving electromagnetic absorption properties at gigahertz frequencies
Authors(s)	Bandaru, Sateesh, Murthy, Narashima, Kulkarni, Ravindra, English, Niall J.
Publication date	2021-09-30
Publication information	Bandaru, Sateesh, Narashima Murthy, Ravindra Kulkarni, and Niall J. English. “Magnetic Ferrite/Carbonized Cotton Fiber Composites for Improving Electromagnetic Absorption Properties at Gigahertz Frequencies.” Elsevier, September 30, 2021. https://doi.org/10.1016/j.jmst.2021.01.041.
Publisher	Elsevier
Item record/more information	http://hdl.handle.net/10197/26138
Publisher's statement	This is the author’s version of a work that was accepted for publication in Journal of Materials Science and Technology. Changes resulting from the publishing process, such as peer review, editing, corrections, structural formatting, and other quality control mechanisms may not be reflected in this document. Changes may have been made to this work since it was submitted for publication. A definitive version was subsequently published in Journal of Materials Science and Technology (86, (2021)) https://doi.org/10.1016/j.jmst.2021.01.041
Publisher's version (DOI)	10.1016/j.jmst.2021.01.041
Notes	Authors listed according to version of record

Downloaded 2026-05-02 00:26:44

The UCD community has made this article openly available. Please share how this access benefits you. Your story matters! (@ucd_oa)

© Some rights reserved. For more information

Magnetic Ferrite / Carbonised Cotton Fibre Composites for Improving Electromagnetic Absorption Properties at Gigahertz Frequencies

Sateesh Bandaru[a,]*, Subramaniam Jayabal[b], Ravindra Kulkarni[c] and Niall J English[a]*

[a] School of Chemical and Bioprocess Engineering, University College Dublin, Belfield, Dublin 4, Ireland.

[b]Center for Green Innovation, School of Mathematics and Physics, University of Science and Technology Beijing, Beijing 100083, China

[c] BVDU's Poona College of Pharmacy, Erandawane, Pune, India

*Corresponding authors: Tel: +353-1-7161921 (BS), E-Mail: Email: sateeshpatrudu@gmail.com, niall.english@ucd.ie

ABSTRACT

Ferrite/carbon composited materials, especially the bio-derived composited materials possessing both environmental friendliness and outstanding microwave absorption performance, attract numerous attention for solving the "electromagnetic problem" in the Gigahertz frequency range. In this work, we demonstrate a bio-derived ferrite/carbon material by compositing functional carbonized cotton fibres (CCFs) and Fe_3O_4 nanoparticles with optimized microwave-absorption properties. By adjusting the carbonization conditions systematically, the Fe_3O_4 loading contents and the microwave absorption properties can be varied simultaneously – and, indeed, optimized and tuned. The CCFs-Fe_3O_4 composites exhibited a minimum reflection-loss capacity *RL*(dB) of -56.8 dB at 10.9 GHz with a thickness of 1.67 mm, and its effective absorption bandwidth (*RL*(dB) <-20 dB) was found to broaden to 7.1 GHz. Electromagnetic characterizations, coupled with microstructure analyses, revealed that the enhancement in microwave absorption was triggered by the different microstructures of CCFs-Fe_3O_4 composites - attributable to the different carbonization processes. These different conditions result in different amounts of Fe_3O_4 attachment sites and lead to the enhancement of dielectric polarisation at localized microstructures. The present work of bio-derived ferrite/carbon materials has important implications in understanding structure-performance relationships in dielectric-magnetic materials, and, meanwhile, could well be extended to a microwave-absorber design approach.

KEYWORDS: Electromagnetic absorption, bio-derived material, dielectric-magnetic composite, interfacial polarisation

Introduction

In the past decade, electromagnetic problems - such as electromagnetic interference and pollution arising from applications in high-frequency technology - have become the main hazards to human health and aggravations to the quality of electronic communication[1-5]. In terms of electromagnetic-absorbing materials for attenuation of electromagnetic intensity as a means to tackle these problems, ferrites are most frequently used as owing to their cost effectiveness, excellent magnetic-loss properties, and good stability [6]. In this context, Yan *et al.* [7-9] have advanced the coordinated co-doping theory of multi-ions in ferrite, leading to the invention of power ferrites with the great scope and promise for the deployment of applications in the MHz-frequency band. Since then, various oxides have been investigated to further improve high-frequency performance [10]. It has been found that the single-phase structure, with refined single-domain grains, has been proven to serve as a prerequisite for high-frequency performance. Moreover, compositing ferrite with dielectric materials, such as ferrite/carbon,[11, 12] and ferrite/polymer[13, 14], has shown excellent microwave-absorption performance in the Gigahertz frequency range. In such composite materials, microwave-absorption properties will be increased by integrating the dielectric loss (complex permittivity, $\varepsilon_r=\varepsilon'$-i$\varepsilon''$), magnetic loss (complex permeability, $\mu_r=\mu'$-iμ''), and impedance matching between these [15-17]. In addition, the microwave-absorption properties of composite microwave-absorption materials, in particular the dielectric-loss capacity, could be further enhanced by substituting heteroatoms in the absorbents, to manipulate the electric-dipole polarisation behavior [18-22]. For example, Li *et al.* [23] reported that the microwave-absorption performance of Fe@C nanocapsules could be increased remarkably after substituted sulfur heteroatoms, ascribed to the formation of -C-S-C- and -C=S- heterostructures. Li *et al.* [24] synthesized the SiC doped Ni@C nanocapsules and found that the minimum reflection loss RL(dB) could reach -49.99 dB at 5.12 GHz.

Although the microwave-absorption properties of such composited absorbents have been increased; however, the developments and applications are also hindered by several bottlenecks, such as high cost, complicated preparation approaches, and environment pollution [25, 26]. Thus, to overcome such blocks and increase microwave-absorption performance, carbonized bio-derived materials, such as cotton, wood, plant leaves, nutshell, and wheat straw, have been employed to act as dielectric-loss materials due to their low cost, favorable renewable-energy footprint, non-toxicity, lightweight nature, and environment-friendly performance [27-30]. Meanwhile, bio-derived materials also contain naturally multiple substituted elements, such as sulfur, nitrogen, phosphorus, and oxygen, which can serve to improve polarisation performance for multiple properties and result in the enhancement of dielectric-loss capacity. Hence, to leverage fully the advantages of bio-derived material and further modify their microwave-absorption properties, we demonstrate in the present work a bio-derived dielectric-magnetic material with compositing functional carbonized cotton fibres (CCFs) and Fe_3O_4 nanoparticles. Notably, we find that microwave-absorption properties can be optimized and tuned by adjusting the carbonized conditions, attributed to the transformation of Fe_3O_4-loading contents and surface/interfacial microstructures of composite materials. In particular, for CCFs-Fe_3O_4 carbonized at 800 ^{o}C for 80 min, its minimum reflection loss capacity RL(dB) reaches -56.8 dB at 10.9 GHz with a thickness of 1.67 mm, and its effective absorption bandwidth (*RL*(dB) <-20 dB) is broadened to 7.1 GHz, exhibiting improved microwave-absorption properties.

Results and discussion

Microstructure characterisation

Carbonized cotton fibres (CCFs) were treated at 700 °C and 800 °C for 80 min and 120 min, respectively, labeled as 700_{80}, 700_{120}, 800_{80}, and 800_{120}. The composite CCFs-Fe_3O_4 were obtained by a hydrothermal method, which is outlined in some detail in the Experimental Section. **Fig. 1a** illustrates the X-ray diffraction patterns of different CCFs-Fe_3O_4 samples, verifying that all of them are composed of the Fe_3O_4 phase. Meanwhile, as the CCFs-Fe_3O_4 is synthesised from a carbon-based skeleton, leading to a localized enlarged pattern exhibited in **Fig. S1**, which demonstrates the (006) peak of carbon fibres at ~26°. It can be discovered that different samples exhibit different intensity values, revealing that the degree of graphitisation and evolution of surface states have been changed after the carbonisation process. To further confirm the extent of graphitisation and intensity of defects, Raman spectra were employed as shown in **Fig. 1b** and **c**. For carbon-based materials, two peaks - the so-called D and G peaks - have always been observed. The D peak centered at ~1,350 cm^{-1} was found to originate from the defective sp^3 bonds and the breathing mode of sp^2 bond in rings, whilst the G peak centered at ~1,580 cm^{-1} originates from the sp^2 bonds [31, 32]. Furthermore, the ratio between I_D and I_G is usually set as a function of defect intensity for carbon-based materials. Assisted by the I_D/I_G values, the concentration of defect sites (n_D) was calculated by **Eq. (1)** [33, 34]:

$$n_D(cm^{-2}) = \frac{(1.8 \pm 0.5) \times 10^{22}}{\lambda^4} \times (\frac{I_D}{I_G}) \qquad (1)$$

in which λ (in nm) represents the wavelength of the Raman laser. For 700_{80}, 700_{120}, 800_{80}, and 800_{120} samples, the I_D/I_G and n_D values were found to be 0.98, 0.96, 1.03, 0.90 and 2.20×10^{11}, 2.15×10^{11}, 2.32×10^{11}, 2.02×10^{11}, respectively. Under different carbonisation conditions, it could be realised that the defect intensity for different samples exhibits a slight difference. In particular, the CCFs-Fe_3O_4 composites which are carbonised under 80 minutes exhibit higher defect intensity than in 120 minutes. Such a different defect intensity could result from different carbonisation conditions, whilst the cotton fiber could convert more completely into carbon fibers when increasing the processing time, and thus increases the extent of graphitisation and decreasing defect intensity. Moreover, comparing with other carbon-based materials [19, 21, 23, 35-43], it should be noted that the defect intensity of CCFs-Fe_3O_4 composites are close to those of rGO, GO, and defective graphite/graphene materials - indicating a relatively high defect intensity in CCFs, triggered by heteroatom substitutions and vacancy defects.

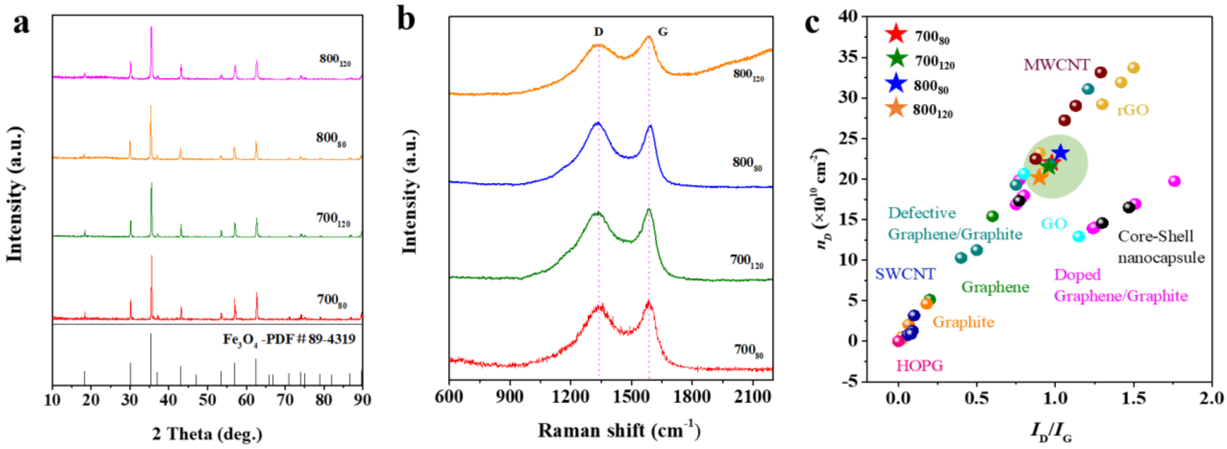

Fig. 1 Characterisations of CCFs-Fe_3O_4 composite. (a) XRD illustration, (b) Raman spectra, and (c) I_D/I_G values vs. n_D of different composites.

The microstructures were characterised initially using a scanning electron microscope (SEM), coupled with an energy-dispersive X-ray spectrum (EDX). SEM and high-resolution SEM images shown in **Fig. 2** confirm similar coating structures for four CCFs-Fe_3O_4 composites. From the HR-SEM images in **Fig. 2e-h**, it has been proven clearly that the attachment quantity for Fe_3O_4 nanoparticles exhibits a distinct difference. The CCFs samples which are carbonised for 80 minutes were found to exhibit relatively sparse nanoparticle-loading structures with numerous “banded” structures emerging at the surface. Furthermore, it can be noted that the cotton fibre has transformed into a twist shape with a diameter of ~8 μm after a carbonised process. Such microstructural difference could be associated with the different extent of graphitisation of CCFs materials under different carbonised conditions, in which the Fe_3O_4 binding sites on the CCFs surfaces have been modified and thus result in the changes of Fe_3O_4 nanoparticle-loading contents. Meanwhile, the EDX-mapping images were employed to reveal the distributions of C (red), O (yellow), and Fe (cyan) in one individual fibre, as shown in **Fig. 2i-l**. It can be noted that the CCFs are coated by Fe_3O_4 nanoparticles, in which the oxygen atoms not only exist in the Fe_3O_4 nanoparticles but also substituted in the CCFs materials. Meanwhile, the magnetic properties would be changed with different Fe_3O_4-loading contents. As the VSM results show in **Fig. 3**, the magnetic property, especially the saturation magnetisation performance (M_S), has been reduced under 80 minutes for the carbonisation process. Such behaviour owes to lower Fe_3O_4-loading contents, which have been revealed in SEM images.

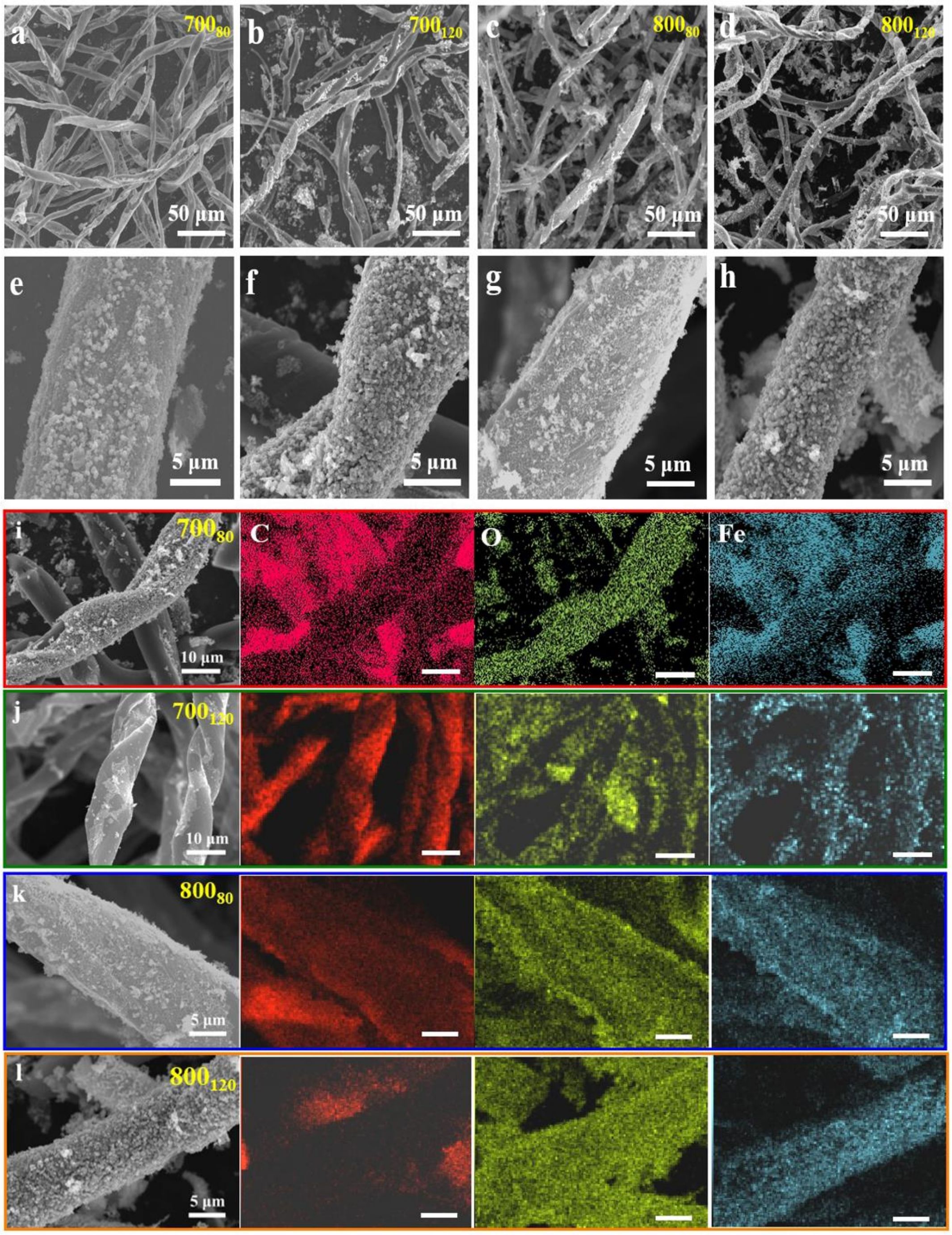

Fig. 2 Microstructures of CCFs-Fe_3O_4 composites. (a)-(d) SEM images of 700_{80}, 700_{120}, 800_{80}, and 800_{120} samples, (e)-(f) The corresponding high-resolution images, (i)-(l) The corresponding elemental C, O, and Fe mapping

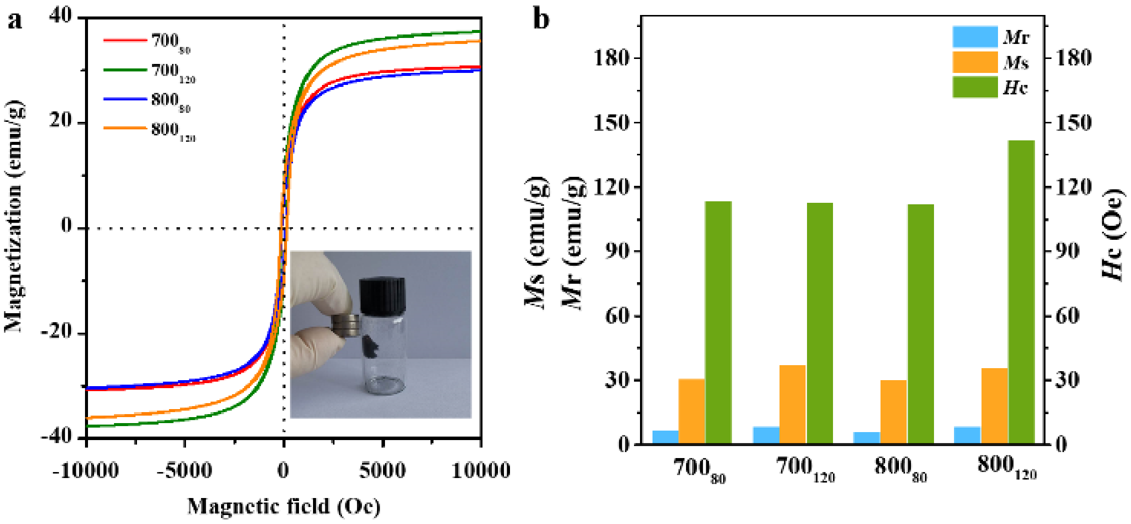

Figure 3. Magnetic properties of CCFs-Fe_3O_4 composite. (a) Magnetic hysteresis loops, (b) Comparison of M_S, M_r, and H_C.

The binding states and elemental distributions of different CCFs-Fe_3O_4 composites are investigated by X-ray photoelectron spectroscopy (XPS) analyses, as shown in **Fig. 4** and **5**. Although the original cotton fibres could contain several different elements, in the present system it can be mainly detected as carbon, oxygen, nitrogen in CCFs and iron, oxygen in Fe_3O_4 (**Fig. 4a** and **4c**). Based on XPS spectra, the binding states for C1s, O1s, and Fe2p have been investigated through software shown in **Fig. 5**. For O1s and Fe2p peaks, the spectra could be divided into Fe-O (O-Fe2$p_{3/2}$ and O-Fe2$p_{1/2}$) for Fe_3O_4 nanoparticles and O=C, O-C for CCFs skeletons. Moreover, the relatively elemental content for different composites has been summarised in **Fig. 4f**. It was found that the composite undergoing carbonisation for 80 minutes contained a lower oxygen content and higher carbon content, especially in the case of the 800 ^{o}C-carbonised composites, which could be attributed to the “banded” structures directly exposing inner CCFs skeleton in the XPS detection. Except for the carbon and oxygen contents, the substituted nitrogen elements exhibit slight changes for different samples, indicating little influence on microwave-absorption property.

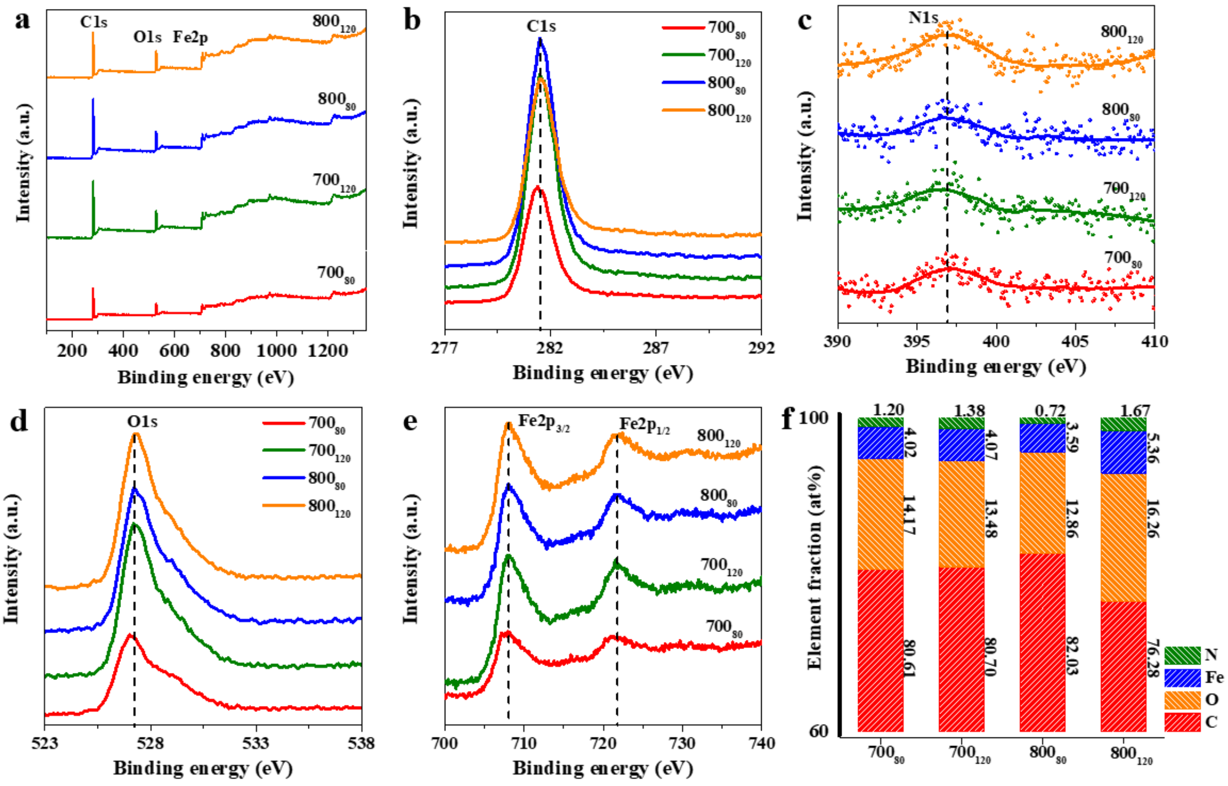

Fig. 4 XPS characterisations of CCFs-Fe$_3$O$_4$ composite. (a) Survey spectra, (b) C1s spectra, (c) N1s spectra, (d) O1s spectra, (e) Fe2p spectra, and (f) The elemental content of different samples.

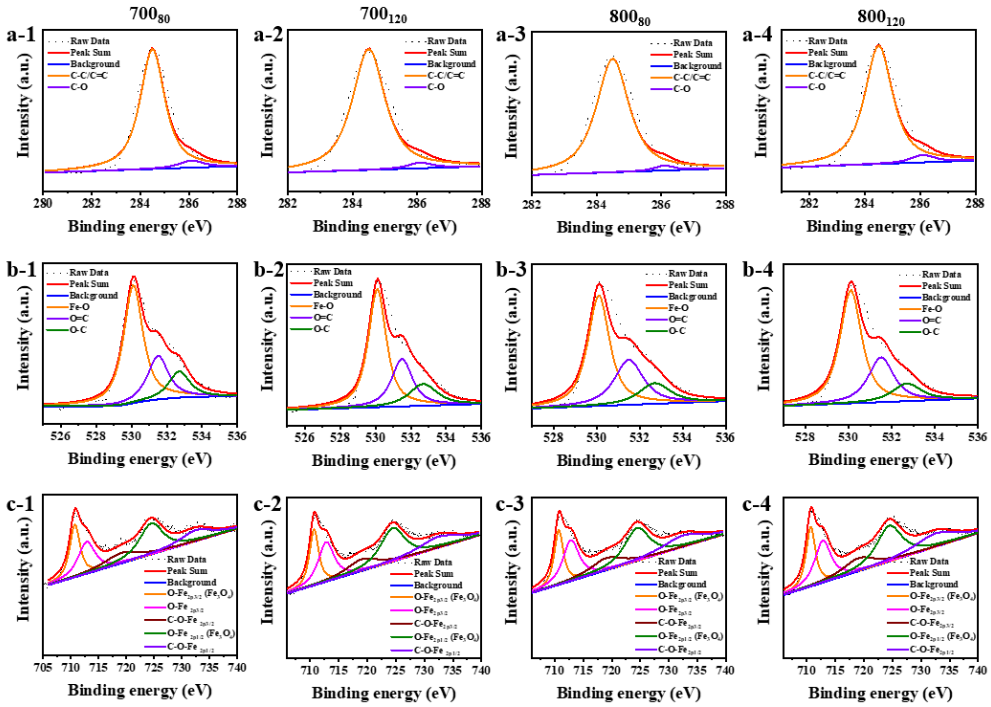

Figure 5. XPS characterisations of CCFs-Fe$_3$O$_4$ composite with peak-fitting. (a) C1s spectra, (b) O1s spectra, (c) Fe2p spectra

Electromagnetic properties

To investigate the microwave absorption properties of CCFs-Fe_3O_4 composites, S-parameters (S_{11} and S_{21}), which represent the reflection (R) and transmission (T) coefficients, have been evaluated by a vector network analyser (VNA) at 2-18 GHz. The absorption (A) coefficient which represents the absorption ability of different samples is calculated by **Eq. (2)** via S-parameters [44, 45].

$$A = 1 - |S_{11}|^2 - |S_{21}|^2 \qquad (2)$$

As shown in **Fig. 6**, for R values, the 700_{120}, 800_{80}, 800_{120}, the composites exhibit resonance peaks at 14.44, 11.08, and 13.56 GHz, respectively, in which the 800_{120} composites provide the deepest resonance intensity amongst the four samples. For T values, the 800_{80} composites were found to exhibit the lowest transmission performance amongst all four samples, and its coefficients exceed -20 dB above 16 GHz. For A values, it can be realised that the 800_{80} composites exhibit a relatively high absorption performance before ~11 GHz, and the 800_{120} composites display an optimised property at 11-18 GHz. This correlation phenomenon may be rationalised by the combination of reflection and transmission behavior, in which the 800_{80} composites were found to exhibit the lowest S_{21} values, whilst the 800_{120} composites present the deepest S_{11} resonance intensity, according to the calculated equation of the microwave-absorption coefficient.

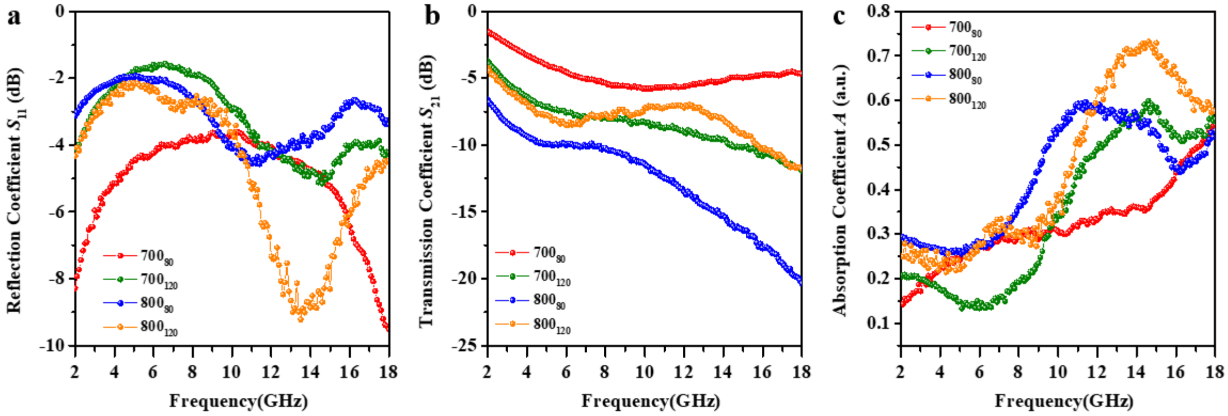

Fig. 6 Scattering parameters of CCFs-Fe_3O_4 composite. (a) Reflection coefficient (S_{11}), (b) Transmission coefficient (S_{21}), (c) Absorption coefficient (A).

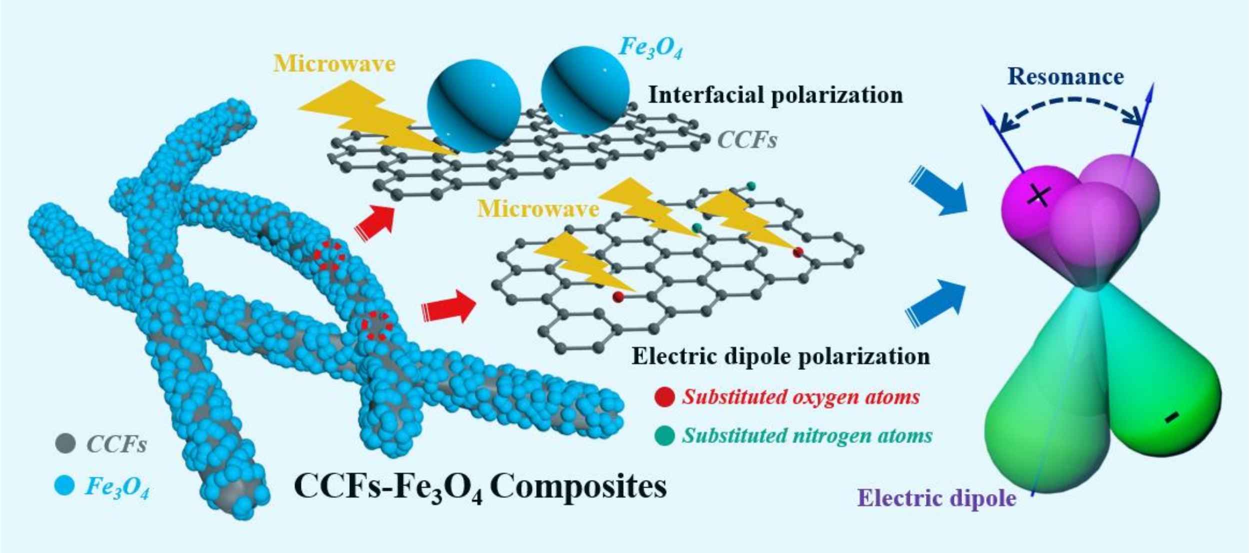

Fig. 7 Scheme of multi-polarisation behaviour, such as interfacial polarisation and electric-dipole polarisation of 800_{80} composites.

To study in detail studied the electromagnetic-response performance for different samples, the relative complex permittivity (ε', ε'') and permeability (μ', μ'') were calculated form S-parameters by N1500A software (Keysight), as shown in **Fig. S2**. It is clear that 800_{80} displays the largest ε' and ε'' values amongst the four samples, in which the ε' and ε'' correspond to the ability to store energy and dielectric loss, respectively. The enhancement of dielectric-loss capacity could be associated with the surface microstructural difference caused by carbonisation, especially the non-dense Fe_3O_4 coating structure ("banded" structure) which has been observed in HR-SEM image. Such a "banded" structure provides an inlet for microwave energy propagating in CCFs skeletons and further creates multi dielectric polarisation sites at the junction between CCFs skeleton and Fe_3O_4 nanoparticle. Furthermore, the electric dipole would also be formed at natural heteroatom substituted sites such as oxygen and nitrogen elements. Under the external electromagnetic field, such dielectric polarisation behaviour serves to offset electromagnetic energy at a specific frequency, resulting in the enhancement of macroscopic dielectric-loss capacity. Consequently, in 800_{80} composites, the electric dipole polarisation was found to be strengthened, owing to more microwave energy entering the interior of CCFs materials for dissipation through "banded" structures. This corresponding, specific loss behaviour is been illustrated in **Fig. 7**. In addition, to further understand the polarisation behaviour, the behaviour of Debye dipole polarisation - based on Cole-Cole "semicircle plots" - has been employed [46]:

$$\varepsilon_r = \varepsilon_\infty + \frac{\varepsilon_s - \varepsilon_\infty}{1 + j2\pi f\tau} = \varepsilon'(f) + i\varepsilon''(f) \qquad (3)$$

$$\varepsilon'(f) = \varepsilon_\infty + \frac{\varepsilon_s - \varepsilon_\infty}{1 + (2\pi f)^2\tau^2} \qquad (4)$$

$$\varepsilon''(f) = \frac{2\pi f\tau(\varepsilon_s - \varepsilon_\infty)}{1 + (2\pi f)^2\tau^2} \qquad (5)$$

where τ is the relaxation time, f is frequency, ε_s and ε_∞ stand for the stationary and optical dielectric constant, respectively. By integrating **Eq. (4)** and **(5)**, we obtain:

$$\varepsilon' = \frac{\varepsilon''}{2\pi f\tau} + \varepsilon_\infty \qquad (6)$$

From **Eq. (6)**, it can be concluded that if dielectric loss is only influenced by electric-dipole polarisation, the plot of ε' verses (ε''/f) would be linear (**Fig. 8**). Each curve can be fitted by lines of different slopes - equal to the frequencies of Debye polarisations f_r. It can be noted that the polarisation behaviour for CCFs-Fe_3O_4 composites could be divided into two parts: low-frequency polarisation (0.5-5 GHz) and high-frequency polarisation (5-40 GHz). Such polarisation phenomena can be rationalised as follow: (1) The π electrons in the material matrix lead to an asymmetric distribution of local electrons, thus forming an intrinsic dielectric polarisation at low frequencies [47-49]; (2) The natural N, P, S, O elements in CCFs, which are substituted originally in carbon fibres during carbonisation, result in a redistribution of charges to form electric dipoles [23], and (3) Strong interface polarisation at the junction between Fe_3O_4 and CCFs [50], which occur at high frequencies. Moreover, for the magnetic loss capacity of different composites, the real and imaginary parts of the complex permeability depict a slight fluctuation. This implies that permeability depends mainly on Fe_3O_4 nanoparticles, but contains a limit on loading content.

Based on this “transmit-line” theory, the reflection-loss capacity, *RL*(dB), versus frequency and thickness, can be expressed as **Eq. (7)**: [51, 52]

$$\mathrm{R(dB)} = 20\lg\left|\frac{\mathrm{Z_{in}}-1}{\mathrm{Z_{in}}+1}\right| \qquad (7)$$

in which the normalised input impedance (Z_{in}) of the absorber can be presented as **Eq. (8)**: [52, 53]

$$Z_{in} = \sqrt{\frac{\mu_r}{\varepsilon_r}}\tanh i\,\frac{2\pi f}{c}\sqrt{\mu_r\varepsilon_r}d \qquad (8)$$

where *c* is the speed of light in free space, *f* is frequency, and *d* is the thickness of the absorber. When *RL*(dB) is less than -20 dB, this indicates that more than 99% of electromagnetic energy has been dissipated. The corresponding frequency range for *RL*(dB) <-20 dB can be regarded as an effective absorption bandwidth. As **Fig. 9** shows, the effective absorption bandwidth for 700_{80}, 700_{120}, 800_{80}, and 800_{120} is 6.5 GHz, 6.6 GHz, 7.1 GHz, and 3.4 GHz, which centered at 8.5-13.6 GHz and 15.5-16.9 GHz, 5-11.6 GHz, 4.4-11.5 GHz, and 4.4-7.8 GHz, respectively. The minimised *RL*(dB) values for four composites correspond to -61.05 dB, -47.72 dB, -56.81 dB, and -34.37 dB at 10.9 GHz, 6.7 GHz, 10.9 GHz, and 6.9 GHz, respectively. It is clear that the microwave absorption properties for 800_{80} composites, especially the effective absorption bandwidth, have been enhanced by structural differences arising from the carbonisation process.

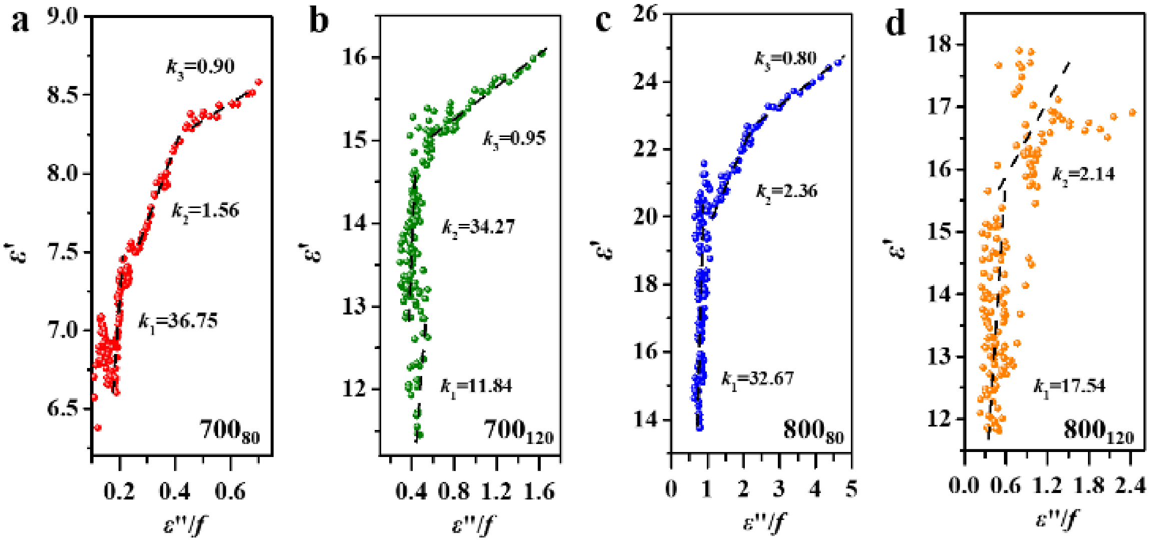

Figure 8. Cole-Cole plots of ε’ versus ε”/f for CCFs-Fe_3O_4 composites.

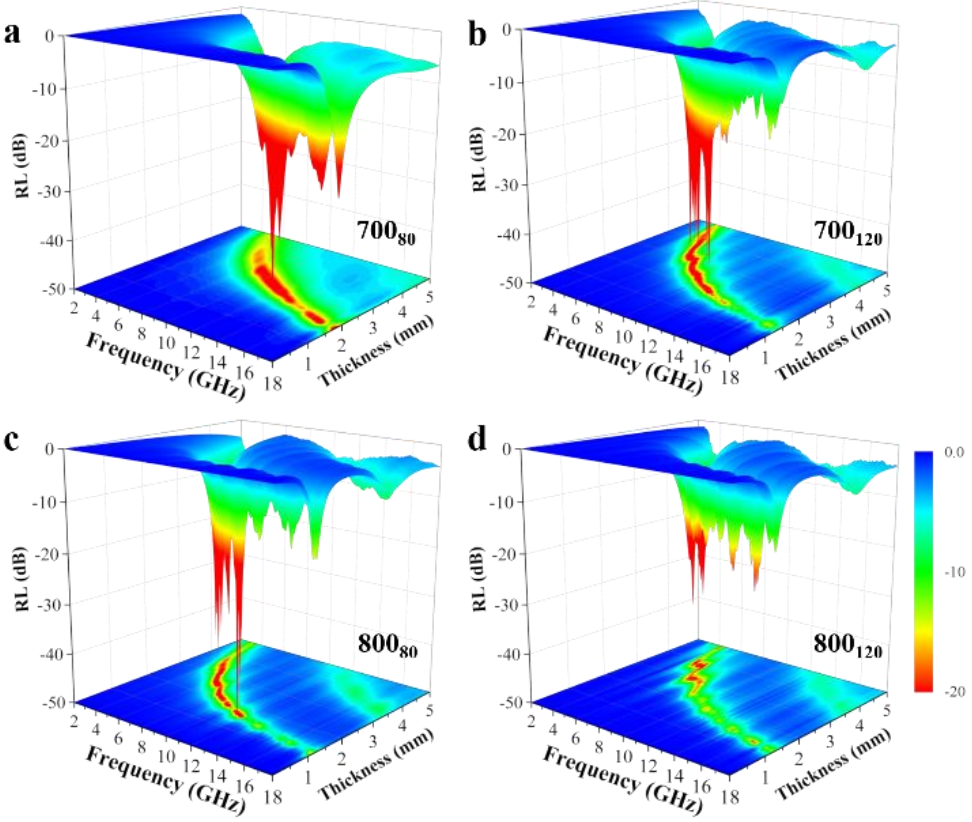

Fig. 9 3D plots of microwave absorption (*RL-f-d*) for CCFs-Fe$_3$O$_4$ composites. (a) 700$_{80}$ composites, (b) 700$_{120}$ composites, (c) 800$_{80}$ composites, (d) 800$_{120}$ composites.

Moreover, the level of impedance matching, Δ, has been determined by **Eq. (9)-(11)** and is exhibited in **Fig. 10**. [54, 55]

$$\Delta = |\sinh^2(kfd) - M| \tag{9}$$

$$k = \frac{4\pi}{c}\sqrt{\varepsilon'\mu'}\frac{\sin(\frac{\delta_E+\delta_M}{2})}{\sqrt{\cos(\delta_E)\cos(\delta_M)}} \tag{10}$$

$$M = \frac{4\varepsilon'\cos(\delta_E)\mu'\cos(\delta_M)}{\left(\mu'\cos(\delta_E)-\varepsilon'\cos(\delta_M)\right)^2(1+\tan^2(\frac{\delta_M-\delta_E}{2}))} \tag{11}$$

where δ_E and δ_M represent the dielectric-loss angle and magnetic loss angle respectively. The matching degree $\Delta < 0.4$ represents that the material contains good impedance matching. It is found that 800_{80} composite contains a relatively small Δ value in lower thickness among all 2-18 GHz than other composites, indicating a better impedance matching performance. It thus evidences that the microwave absorption property could be improved by the structural differences arising from carbonised conditions.

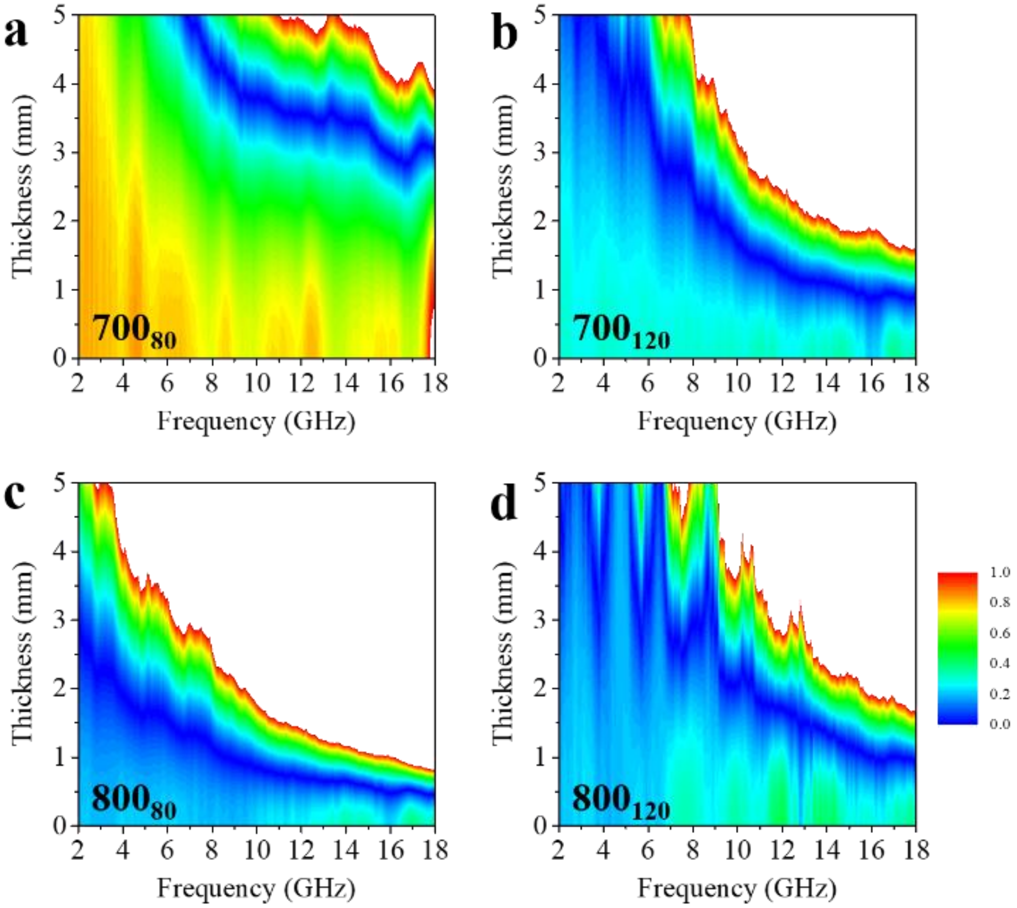

Figure 10. Impedance-matching degree Δ: dependence on frequency for the CCFs-Fe_3O_4 composites.

Conclusion

In summary, we have prepared a bio-derived dielectric-magnetic material by compositing carbonised cotton fibres (CCFs) and Fe_3O_4 nanoparticles, in which the CCFs have been carbonised at different temperatures and for different periods. Experimental results provide direct evidence for the microstructures and electromagnetic characterisations could be optimsied and ‘tuned’ by adjusting carbonised conditions. Attributing to the “banded” structures, heteroatom substitutions, and Fe_3O_4 coatings, the dielectric-loss capacity has been increased at 2-18 GHz, ascribed to the enhancement of dielectric polarisation at such localised microstructures. In particular, 800_{80} composites exhibits the optimised RL(dB) of -56.8 dB at 10.9 GHz with a thickness of 1.67 mm, and its effective absorption bandwidth (RL(dB) <-20 dB) is broadened to 7.1 GHz. Considering the abundant natural resources, the present work not only proposes a new understanding of the structure-activity relationship but provides a new type of eco-friendly, high-performance microwave absorbers.

Experimental Methods

Preparation of carbon cotton fibres (CCFs) The natural cotton was placed in a ceramic boat and then respectively heated to 700^oC and 800^oC in a quartz tube with a heating rate of 10 ^oC/min in Ar atmosphere. The annealed time was set at 80 min and 120 min, respectively. The obtained CCFs samples were labeled as 700_{80}, 700_{120}, 800_{80}, and 800_{120} in the following sections.

Preparation of CCFs-Fe_3O_4 composite Fe_3O_4 nanoparticles were prepared by a hydrothermal method [56]. Firstly, 4 mmol of $FeSO_4{\cdot}7H_2O$ was dissolved in 15 mL deionised water. After stirring (600 rpm) for 30 min, the solution was transferred into a Teflon-lined stainless-steel autoclave with a volume of 50 mL. Then, 4 mL of $N_2H_4{\cdot}H_2O$ and 4 mL of $NH_3{\cdot}H_2O$ were added into the above solution. The solution pH value was adjusted to ~11. Then, the CCFs were added into the mixed solution. After the reaction was carried out at 150 ^{o}C for 15 h in the oven, the system was naturally cooled to room temperature. The black precipitate was washed with deionised water and absolute ethanol several times. Finally, the prepared product was dried at 60 ^{o}C for 12 h.

Microstructure characterisations The crystal structure of the CCFs-Fe_3O_4 was detected by X-ray diffraction (XRD) using CuK_α radiation (λ=0.154 nm). The morphology and elemental mapping were characterised by a scanning electron microscope (SEM) and energy-dispersive X-ray spectrum (EDS) (JEOL JSM-7001F field-emission scanning electron microscope). Raman spectra were recorded by a LabRAM HR Raman microscope with a laser wavelength of 532 nm. The surface element and chemical state were analysed by an X-ray photoelectron spectroscopy (XPS, Phoibos 100 spectrometer). The magnetic hysteresis loops were measured on a vibrating sample magnetometer (VSM, Lakeshore 7307) with a maximum magnetic field of 10 kOe at room temperature.

Electromagnetic measurements Electromagnetic parameters and scattering parameters (*S*-parameters) were measured by a vector network analyser (Keysight N5222A), which was calibrated by 2 port short-open-load-thru (SOLT) calibration standard (85054B) with a Type-N 50 Ω coaxial airline [57]. CCFs-Fe_3O_4 composites were mixed uniformly with paraffin at a weight percentage of 30 wt.%, and then processed to a toroidal shape of 7.00 mm outer diameter and 3.04 mm inner diameter.

AUTHOR INFORMATION

Author Contributions

All authors have agreed to the manuscript.

Notes

There are no conflicts of interest to declare.

Acknowledgments

The authors gratefully acknowledge the National Natural Science Foundation of China (U1704253), the Fundamental Research Funds for the Central Universities (N160208001, N180206001), the Zhejiang provincial natural science foundation of China (LR18E010001), Science Foundation Ireland (SFI 17/NSFC/5229) as part of the bilateral Ireland-China SFI-NSFC programme, the LiaoNing Revitalisation Talents Program (XLYC1807177), the national 1000-plan for young scholars and the start-up funding supported from the Northeastern University of China.

References

1. Guo, J.; Morris, J. R.; Ihm, Y.; Contescu, C. I.; Gallego, N. C.; Duscher, G.; Pennycook, S. J.; Chisholm, M. F., Topological defects: origin of nanopores and enhanced adsorption performance in nanoporous carbon. *Small* **2012,** *8* (21), 3283-3288.
2. Li, W.; Li, C.; Lin, L.; Wang, Y.; Zhang, J., Foam structure to improve microwave absorption properties of silicon carbide/carbon material. *J. Mater. Sci. Technol.* **2019,** *35* (11), 2658-2664.
3. Huang, Z.; Chen, H.; Huang, Y.; Ge, Z.; Zhou, Y.; Yang, Y.; Xiao, P.; Liang, J.; Zhang, T.; Shi, Q., Ultra-broadband wide-angle terahertz absorption properties of 3D graphene foam. *Adv. Funct. Mater.* **2018,** *28* (2), 1704363.
4. Xu, J.; Liu, J.; Che, R.; Liang, C.; Cao, M.; Li, Y.; Liu, Z., Polarisation enhancement of microwave absorption by increasing aspect ratio of ellipsoidal nanorattles with Fe_3O_4 cores and hierarchical $CuSiO_3$ shells. *Nanoscale* **2014,** *6* (11), 5782-5790.
5. Singh, P., Babbar, V. K., Razdan, A., Puri, R. K., Goel, T. C., Complex permittivity, permeability, and x-band microwave absorption of cacoti ferrite composites. *J. Appl. Phys.* **2000**, 87(9), 4362-4366.
6. Yi S. B., Bai G. H., Wang X. Y., Zhang X. F., Hussain A., Jin J. Y., Yan M., Development of high-temperature high-permeability MnZn power ferrites for MHz application by Nb_2O_5 and TiO_2 co-doping, *Ceram. Int.* **2020**, 46, 8935-8941.
7. Hussain A., Bai G. H., Huo H. X., Yi S. B., Wang X. Y., Fan X. Y., Yan M., Co_2O_3 and SnO_2 doped MnZn ferrites for applications at 3-5 MHz frequencies, *Ceram. Inter.* **2019**, 45, 12544-12549.

8. Yan M., Hu J., Luo W., Zhang W. Y., Preparation and investigation of low firing temperature NiCuZn ferrites with high relative initial permeability, *J. Magn. Magn. Mater.* **2006** 303, 249-255.
9. Hussain A., Naeem A., Bai G. H., Yan M., Structural, dielectric and magnetic studies of cobalt ferrite nanoparticles for selected annealing temperatures, *J. Mater. Sci.-Mater. Elec.* **2018**, 29, 20783-20789.
10. Yang, N.; Zeng, J.; Xue, J.; Zeng, L.; Zhao, Y., Strong absorption and wide-frequency microwave absorption properties of the nanostructure zinc oxide/zinc/carbon fibre multilayer composites. *J. Alloy. Compd.* **2018,** *735*, 2212-2218.
11. Liu, D.; Qiang, R.; Du, Y.; Wang, Y.; Tian, C.; Han, X., Prussian blue analogues derived magnetic FeCo alloy/carbon composites with tunable chemical composition and enhanced microwave absorption. *J. Colloid Interf. Sci* **2018,** *514*, 10-20.
12. Wu, T.; Liu, Y.; Zeng, X.; Cui, T.; Zhao, Y.; Li, Y.; Tong, G., Facile hydrothermal synthesis of Fe_3O_4/C core–shell nanorings for efficient low-frequency microwave absorption. *ACS Appl. Mater. Interfaces* **2016,** *8* (11), 7370-7380.
13. Zhang, X.; Li, Y.; Liu, R.; Rao, Y.; Rong, H.; Qin, G., High-magnetisation FeCo nanochains with ultrathin interfacial gaps for broadband electromagnetic wave absorption at gigahertz. *ACS Appl. Mater. Interfaces* **2016,** *8* (5), 3494-3498.
14. Tian, X.; Meng, F.; Meng, F.; Chen, X.; Guo, Y.; Wang, Y.; Zhu, W.; Zhou, Z., Synergistic enhancement of microwave absorption using hybridised polyaniline@helical CNTs with dual chirality. *ACS Appl. Mater. Interfaces* **2017,** *9* (18), 15711-15718.
15. Li, Y.; Gao, T.; Zhang, W.; Hu, H.; Rong, H.; Zhang, X., Fe@CN_x nanocapsules for microwave absorption at gigahertz frequency. *ACS Appl. Nano Mater.* **2019,** *2* (6), 3648-3653.
16. Yin, Y.; Liu, X.; Wei, X.; Li, Y.; Nie, X.; Yu, R.; Shui, J., Magnetically aligned Co–C/MWCNTs composite derived from MWCNT-interconnected zeolitic imidazolate frameworks for a lightweight and highly efficient electromagnetic wave absorber. *ACS Appl. Mater. Interfaces* **2017,** *9* (36), 30850-30861.
17. Liu, D.; Du, Y.; Xu, P.; Liu, N.; Wang, Y.; Zhao, H.; Cui, L.; Han, X., Waxberry-like hierarchical Ni@C microspheres with high-performance microwave absorption. *J. Mater. Chem. C* **2019,** *7* (17), 5037-5046.
18. Zhang, X.; Guo, J.; Guan, P.; Qin, G.; Pennycook, S. J., Gigahertz dielectric polarisation of substitutional single niobium atoms in defective graphitic layers. *Phys. Rev. Lett.* **2015,** *115* (14), 147601.
19. Li, Y.; Liu, X.; Liu, R.; Pang, X.; Zhang, Y.; Qin, G.; Zhang, X., Improved microwave absorption properties by atomic-scale substitutions. *Carbon* **2018,** *139*, 181-188.
20. Xu, Z.; Du, Y.; Liu, D.; Wang, Y.; Ma, W.; Wang, Y.; Xu, P.; Han, X., Pea-like Fe/Fe_3C nanoparticles embedded in nitrogen-doped carbon nanotubes with tunable dielectric/magnetic loss and efficient electromagnetic absorption. *ACS Appl. Mater. Interfaces* **2019,** *11* (4), 4268-4277.
21. Li, Y.; Chen, X.; Wei, Q.; Liu, W.; Zhang, Y.; Qin, G.; Shi, Z.; Zhang, X., Oxygen-sulphur Co-substitutional Fe@C nanocapsules for improving microwave absorption properties. *Sci. Bull.* **2020,** *65* (8), 623-630.
22. Li, Y.; Zheng, Y.; Liu, R.; Rao, Y.; Su, R.; Yu, J.; Liu, X.; Guan, P.; Guo, J.; Zhang, X., Enhanced high-frequency microwave absorption in core-shell nanocapsules with atomic-scale oxygen substitutions. *J. Appl. Phys.* **2020,** *127* (19), 195107.

23. Li, Y.; Liu, R.; Pang, X.; Zhao, X.; Zhang, Y.; Qin, G.; Zhang, X., Fe@C nanocapsules with substitutional sulphur heteroatoms in graphitic shells for improving microwave absorption at gigahertz frequencies. *Carbon* **2018,** *126*, 372-381.
24. Li, Z.; Ding, X.; Li, F.; Liu, X.; Zhang, S.; Long, H., Enhanced dielectric loss induced by the doping of SiC in thick defective graphitic shells of Ni@C nanocapsules with ash-free coal as carbon source for broadband microwave absorption. *J. Phys. D Appl. Phys.* **2017,** *50* (44), 445305.
25. Luo, C.; Tang, Y.; Jiao, T.; Kong, J., High-temperature stable and metal-free electromagnetic wave-absorbing SiBCN ceramics derived from carbon-rich hyperbranched polyborosilazanes. *ACS Appl. Mater. Interfaces* **2018,** *10* (33), 28051-28061.
26. Nazir, A.; Yu, H.; Wang, L.; Haroon, M.; Ullah, R. S.; Fahad, S.; Elshaarani, T.; Khan, A.; Usman, M., Recent progress in the modification of carbon materials and their application in composites for electromagnetic interference shielding. *J. Mater. Sci.* **2018,** *53* (12), 8699-8719.
27. Li, X.; Yang, Y.; Liu, J.; Ouyang, L.; Liu, J.; Hu, R.; Yang, L.; Zhu, M., MoS_2/cotton-derived carbon fibres with enhanced cyclic performance for sodium-ion batteries. *Appl. Surf. Sci.* **2017,** *413*, 169-174.
28. Yuan, Y.; Sun, X.; Yang, M.; Xu, F.; Lin, Z.; Zhao, X.; Ding, Y.; Li, J.; Yin, W.; Peng, Q., Stiff, thermally stable and highly anisotropic wood-derived carbon composite monoliths for electromagnetic interference shielding. *ACS Appl. Mater. Interfaces* **2017,** *9* (25), 21371-21381.
29. Shen, Z.; Feng, J., Preparation of thermally conductive polymer composites with good electromagnetic interference shielding efficiency based on natural wood-derived carbon scaffolds. *ACS Sustain. Chem. Eng.* **2019,** *7* (6), 6259-6266.
30. Li, Z.; Lin, H.; Ding, S.; Ling, H.; Wang, T.; Miao, Z.; Zhang, M.; Meng, A.; Li, Q., Synthesis and enhanced electromagnetic wave absorption performances of Fe_3O_4@C decorated walnut shell-derived porous carbon. *Carbon* **2020,** *167*, 148-159.
31. Dresselhaus, M. S.; Jorio, A.; Hofmann, M.; Dresselhaus, G.; Saito, R., Perspectives on carbon nanotubes and graphene Raman spectroscopy. *Nano Lett* **2010,** *10* (3), 751-758.
32. Ferrari, A. C.; Meyer, J.; Scardaci, V.; Casiraghi, C.; Lazzeri, M.; Mauri, F.; Piscanec, S.; Jiang, D.; Novoselov, K.; Roth, S., Raman spectrum of graphene and graphene layers. *Phys. Rev. Lett.* **2006,** *97* (18), 187401.
33. Cançado, L.; Takai, K.; Enoki, T.; Endo, M.; Kim, Y.; Misusaki, H.; Jorio, A.; Coelho, L.; Magalhaes-Paniago, R.; Pimenta, M., General equation for the determination of the crystallite sise L_a of nanographite by Raman spectroscopy. *Appl. Phys. Lett.* **2006,** *88* (16), 163106.
34. Ferrari, A. C.; Basko, D. M., Raman spectroscopy as a versatile tool for studying the properties of graphene. *Nat. Nanotechnol.* **2013,** *8* (4), 235-246.
35. Bruna, M.; Ott, A. K.; Ijäs, M.; Yoon, D.; Sassi, U.; Ferrari, A. C., Doping dependence of the Raman spectrum of defected graphene. *ACS Nano* **2014,** *8* (7), 7432-7441.
36. Chernyak, S. A.; Ivanov, A. S.; Maslakov, K. I.; Egorov, A. V.; Shen, Z.; Savilov, S. S.; Lunin, V. V., Oxidation, defunctionalisation and catalyst life cycle of carbon nanotubes: a Raman spectroscopy view. *Phys. Chem. Chem. Phys.* **2017,** *19* (3), 2276-2285.
37. Claramunt, S.; Varea, A.; López-Díaz, D.; Velázquez, M. M.; Cornet, A.; Cirera, A., The importance of interbands on the interpretation of the Raman spectrum of graphene oxide. *J. Phys. Chem. C* **2015,** *119* (18), 10123-10129.

38. Eigler, S.; Dotzer, C.; Hirsch, A., Visualisation of defect densities in reduced graphene oxide. *Carbon* **2012,** *50* (10), 3666-3673.
39. Kariminejad, B.; Salami-Kalajahi, M.; Roghani-Mamaqani, H.; Noparvar-Qarebagh, A., Effect of surface chemistry of graphene and its content on the properties of ethylene dichloride-and disodium tetrasulfide-based polysulfide polymer nanocomposites. *Polym. Composite.* **2017,** *38*, E515-E524.
40. Sun, Z.; Yan, Z.; Yao, J.; Beitler, E.; Zhu, Y.; Tour, J. M., Growth of graphene from solid carbon sources. *Nature* **2010,** *468* (7323), 549-552.
41. Vinod, S.; Tiwary, C. S.; Machado, L. D.; Ozden, S.; Vajtai, R.; Galvao, D. S.; Ajayan, P. M., Synthesis of ultralow density 3D graphene–CNT foams using a two-step method. *Nanoscale* **2016,** *8* (35), 15857-15863.
42. Voiry, D.; Yang, J.; Kupferberg, J.; Fullon, R.; Lee, C.; Jeong, H. Y.; Shin, H. S.; Chhowalla, M., High-quality graphene via microwave reduction of solution-exfoliated graphene oxide. *Science* **2016,** *353* (6306), 1413-1416.
43. Zafar, Z.; Ni, Z. H.; Wu, X.; Shi, Z. X.; Nan, H. Y.; Bai, J.; Sun, L. T., Evolution of Raman spectra in nitrogen doped graphene. *Carbon* **2013,** *61*, 57-62.
44. Brosseau, C.; NDong, W.; Mdarhri, A., Influence of uniaxial tension on the microwave absorption properties of filled polymers. *J. Appl. Phys.* **2008,** *104* (7), 074907.
45. Qin, F.; Brosseau, C.; Peng, H.; Wang, H.; Sun, J., In situ microwave characterisation of microwire composites with external magnetic field. *Appl. Phys. Lett.* **2012,** *100* (19), 192903.
46. Zhang, X.; Guan, P.; Dong, X., Multidielectric polarisations in the core/shell Co/graphite nanoparticles. *Appl. Phys. Lett.* **2010,** *96* (22), 223111.
47. Haddon, R. C., Chemistry of the fullerenes: the manifestation of strain in a class of continuous aromatic molecules. *Science* **1993,** *261* (5128), 1545-50.
48. Ugarte, D.; Chatelain, A.; de Heer, W. A., Nanocapillarity and Chemistry in Carbon Nanotubes. *Science* **1996,** *274* (5294), 1897-9.
49. Shan, B.; Cho, K., First-principles study of work functions of double-wall carbon nanotubes. *Physical Review B* **2006,** *73* (8).
50. Cao, M. S.; Yang, J.; Song, W. L.; Zhang, D. Q.; Wen, B.; Jin, H. B.; Hou, Z. L.; Yuan, J., Ferroferric oxide/multiwalled carbon nanotube vs polyaniline/ferroferric oxide/multiwalled carbon nanotube multiheterostructures for highly effective microwave absorption. *ACS Appl Mater Interfaces* **2012,** *4* (12), 6949-56.
51. Li, Y.; Wang, J.; Liu, R.; Zhao, X.; Wang, X.; Zhang, X.; Qin, G., Dependence of gigahertz microwave absorption on the mass fraction of Co@C nanocapsules in composite. *Journal of Alloys and Compounds* **2017,** *724*, 1023-1029.
52. Wang, J.; Wang, Z.; Liu, R.; Li, Y.; Zhao, X.; Zhang, X., Heterogeneous interfacial polarisation in Fe@ZnO nanocomposites induces high-frequency microwave absorption. *Materials Letters* **2017,** *209*, 276-279.
53. Wang, Z.; Liu, X.; Li, Y.; Wang, J.; Liu, R.; Zhang, Y.; Wang, Z.; Yu, J.; Chen, W.; Shi, Z.; Zhang, J.; Zhang, X., Improved microwave absorbing properties by designing heterogeneous interfaces in Mo@2D-MoS2. *Journal of Alloys and Compounds* **2018,** *767*, 1-6.
54. Quan, L.; Qin, F. X.; Estevez, D.; Wang, H.; Peng, H. X., Magnetic graphene for microwave absorbing application: Towards the lightest graphene-based absorber. *Carbon* **2017,** *125*, 630-639.

55. Zhou, Y.; Wang, N.; Muhammad, J.; Wang, D.; Duan, Y.; Zhang, X.; Dong, X.; Zhang, Z., Graphene nanoflakes with optimised nitrogen doping fabricated by arc discharge as highly efficient absorbers toward microwave absorption. *Carbon* **2019,** *148*, 204-213.
56. Yuan, K.; Ni, Y.; Zhang, L., Facile hydrothermal synthesis of polyhedral Fe_3O_4 nanocrystals, influencing factors and application in the electrochemical detection of H_2O_2. *J. Alloy. Compd* **2012,** *532*, 10-15.
57. Brosseau, C.; NDong, W.; Castel, V.; Youssef, J. B.; Vidal, A., Electromagnetomechanical coupling characteristics of plastoferrites. *J. Appl. Phys.* **2007,** *102* (2), 024907.